PCCP

ARTICLE

Spectroscopic identification of the chemical interplay between defects and dopants in Al-doped ZnO

Received 00th January 20xx,
Accepted 00th January 20xx

DOI: 10.1039/x0xx00000x

www.rsc.org/

S. Benedetti[a,†], I. Valenti[a,b], A. di Bona,[a] G. Vinai[c], C. Castan-Guerrero[c], S. Valeri[a,b], A. Catellani[a], A. Ruini[a,b], P. Torelli[c], A. Calzolari[a]

The conduction and optoelectronic properties of transparent conductive oxides can be largely modified by intentional inclusion of dopants over a very large range of concentration. However, the simultaneous presence of structural defects results in an unpredictable complexity that prevents a clear identification of chemical and structural properties of the final samples. By exploiting the unique chemical sensitivity of Hard X-ray Photoelectron Spectra and Near Edge X-ray Absorption Fine Structure in combination with Density Functional Theory, we determine the contribution to the spectroscopic response of defects in Al-doped ZnO films. Satellites peaks in O1s and modifications in the O K-edge allow to determine the presence of H embedded in ZnO and the very low concentration of Zn vacancies and O interstitials in undoped ZnO. Contributions coming from substitutional and (above the solubility limit) interstitial Al atoms have been clearly identified and have been related to changes in the oxide stoichiometry and an increased oxygen coordination, together with small lattice distortions. In this way defects and doping in oxide films can be controlled, in order to tune their properties and improve their performances.

Introduction

Transparent Conducting Oxides (TCO) have gained large interest in the last years because of the peculiar combination of high transparency and low electric resistivity. These oxides are obtained by doping wide-band gap semiconductors – as it happens for the most common and exploited tin-doped indium oxide (ITO) and aluminium-doped zinc oxide (AZO) – and can find applications in optoelectronic and plasmonic devices.[1,2] Increasing efforts are dedicated to the improvement of conductivity and to obtain a high control over carrier density, which are mandatory prerequisite for reliable and efficient devices. Defects and impurities play a key role in the optoelectronic response,[3,4] thus their identification and control is highly desirable. Indeed, it has been extensively shown that the conductivity and doping character of TCO are strictly related to the type and abundance of defects in the system.[5,6] Even when a dopant is intentionally introduced in the oxide to tune the response of the system, still undesired defects present in the sample can interfere, amplify or quench the desired outcome by affecting the adsorption sites and the coordination of the dopants, by imparting not-obvious electron-compensation effects or by including scattering centers/optical traps in the gap.[7,8] Thus, the optoelectronic performances of metal oxides, even with the same formal dopant concentration, strictly depend on the quality of the samples and on the growth techniques.[3,9] The coexistence of high doping level and defects results in disordered structures, whose atomistic and electronic properties may be very different from the ideal crystalline host. This represents a severe limitation for the application of these materials in optoelectronic devices. It is thus becoming increasingly interesting to intentionally control the defect concentration and their role in the final properties of such oxide systems, opening the way to a true defect engineering.

Even for simple and well-studied binary oxides, such as ZnO, TiO_2, SnO_2, the simultaneous inclusion of defects and dopant rapidly increases the complexity (i.e. disorder, inhomogeneity, locality) of the system, making the use of many spectroscopic (e.g. UV-vis, UPS, ARPES), diffraction (e.g. LEED) and microscopic (e.g. STM, AFM) techniques unsuitable for the characterization of the sample. In this sense X-ray based spectroscopies, in combination with their interpretation through first-principles theoretical calculations, are a fundamental tool to control and successively tune the response of such highly defective systems, giving local insights on the chemistry, coordination and composition of the sample. Spectroscopic fingerprints of defective sites must then be recognized and correctly interpreted, as often a simple qualitative interpretation of spectra can be misleading.

In this framework Al-doped ZnO (AZO) has been extensively investigated: being a simple tetrahedral compound, the material is a good candidate to show the potential of spectroscopic identification of defects to unravel the complex

[a] CNR, Istituto Nanoscienze, Via G. Campi 213/a, 41125 Modena, Italy.
[b] Dipartimento di Scienze Fisiche, Informatiche e Matematiche, Università di Modena e Reggio Emilia, via Campi 213/a, 41125 Modena, Italy.
[c] Laboratorio TASC, IOM-CNR, S.S. 14 km 163.5, Basovizza, I-34149 Trieste, Italy.
† corresponding author: stefania.benedetti@nano.cnr.it.

atomic environment modifications induced, and gain a deeper comprehension of the material and its reliable application in devices.[10-12] While defects in undoped ZnO have been extensively investigated,[5,6] few studies on the spectroscopic characterization of defective AZO films have been reported.[15-17] Mainly they report theoretical predictions concerning the stability of different type of vacancies, interstitial atoms or their complexes, and the consequences on electronic properties. However, the interplay between structural defects and impurity dopants is far to be understood and their spectroscopic identification is really poor.[15,18] X-ray Photoelectron Spectroscopy (XPS) of O1s is frequently investigated in order to have an indication of the chemical quality of TCOs. In AZO, the O1s peak is asymmetric because of the presence of additional components besides the contribution coming from O^{2-} in the ZnO wurtzite structure.[19] Additional components located at higher binding energy with respect to the main peak have been assigned for long time to O in O-deficient regions and to contaminants (OH^- in particular).[20,21] More recently contributions from O in the surrounding of dopant have been considered.[22] Near Edge X-ray Absorption Fine Structure (NEXAFS) is usually even more difficult to interpret, because of the many contributions coming into play in spectra, due to the convolution of electronic effects and structural environment.[23] Recently it has been shown that main changes in NEXAFS O-K edge spectra are due to structural modifications.[18] A clear identification of spectroscopic contributions of defects is thus extremely useful for material control.

In this work we present a detailed study of the spectroscopic signatures of main defects present in AZO films, by means of Hard X-ray photoelectron spectroscopy (HAXPES), Near Edge X-ray Absorption Fine Structure (NEXAFS) and their interpretation through first-principles calculations. We demonstrate that sensitivity to element and to the local environment allow us to clearly determine the presence of H incorporation in ZnO, Zn vacancies and Al interstitials in AZO films for a large range of dopant concentration. Our results provide a strong tool for further control and tuning of the optoelectronic properties of the TCO.

Experimental

AZO films of 270 nm thickness have been deposited by magnetron sputtering on a polished MgO(001) substrate. AZO films have been obtained by co-deposition from a 3" RF magnetron source (ZnO) and a 3" DC magnetron source (Al) operating in confocal geometry approximately 15 cm far from the substrate. A constant 0.7 Å/s ZnO deposition rate was reached at RF power of 120 W. The DC power was varied in order to obtain the desired doping level, defined as Al/(Al+Zn). Deposition was performed at room temperature with base pressure of 1×10^{-6} mbar, in a 5×10^{-3} mbar Ar gas atmosphere. A rotating sample holder has been used to obtain a uniform deposition. Doping level has been determined by Energy-Dispersive X-ray Spectroscopy and confirmed by HAXPES.

HAXPES measurements have been performed at Galaxies beamline at Soleil Synchrotron in Paris.[24,25] Spectra have been acquired with fixed photon energy of about 2.5 keV and an overall energy resolution of about 0.15 eV. The beam was impinging on the sample forming an angle of 87° with the normal to the surface and photoelectrons were collected around normal emission. Peak positions are calibrated by measuring the Fermi level in every sample.[12] The X-ray absorption measurements (NEXAFS) were performed in the high energy branch of the APE beamline at Elettra synchrotron, Trieste.[26] We adopted a beamline configuration with 1000 resolving power which ensure 0.5 eV of energy resolution at the O K-edge and roughly 1 eV at the Zn $L_{2,3}$. The linearly polarized light was impinging on the sample forming an angle of 45° with respect to the normal at the surface exactly as the electric vector and the surface normal. The O K-edge spectra obtained from the sample were divided by a spectrum measured in the same conditions on a reference sample of pure gold. Films were transported to synchrotrons in a dryer and always kept in a controlled atmosphere when not measured. No treatment in vacuum was performed prior to the experiments.

Theory

Ground-state electronic structure and geometry optimization for ZnO and its derivatives were performed at the density functional level of theory using the Quantum ESPRESSO software package.[27] All calculations employed the PBE exchange-correlation functional, a plane wave basis set with a kinetic energy cutoff of 28 Ry (280 Ry) for the description of Kohn-Sham orbitals (charge density), and ultrasoft pseudopotentials.[28] The 3d electrons of Zn have been explicitly included in the valence shell. Underestimation of the band gap with standard GGA type functionals was corrected by including a Hubbard-like potential on both 3d orbitals of zinc (U_{Zn}) and 2p orbitals of oxygen (U_O), along the lines described in e.g. Refs 29,30. The optimized values for this compound, U_{Zn} = 12.0 eV and U_O = 6.5 eV, where obtained by means of the pseudohybrid Hubbard Density Functional approach (namely ACBN0), recently proposed by Agapito and coworkers.[31] The effects of the ACBN0 approach on the structural, electronic and vibrational properties of ZnO and AZO, along with chalcogenides and metal oxides have been largely tested in previous reports.[10,16,31,32]

The ZnO and AZO bulk crystals were simulated using periodic supercells, including 16 primitive ZnO wurtzite cells (i.e. 64 atoms). The Brillouin zone of the reciprocal lattice was sampled by using a uniform (4x4x4) grid of k-points. In the sub-solubility limit (Al < 3.5%), Al ions assumed a Zn-substitutional position in the ZnO crystal. For higher Al concentration (4.6%) both substitutional and interstitial sites were considered. Point defects in ZnO and AZO, namely oxygen vacancies (V_O) zinc vacancies (V_{Zn}), oxygen interstitials (O_i) and hydrogen impurities (H), were simulated in the same cell, removing (adding) one specific atom per cell. Interstitial configurations were obtained from 1ps-long Car-Parrinello molecular

dynamics simulations at room temperature.[27] All structures were relaxed until forces on all atoms were lower than 0.03 eV/Å.

The O1s core level shifts (CLSs) are calculated in the pseudopotential formalism, assuming static screening. For a pair of inequivalent atoms (one assumed as a reference), the core-hole binding energy (BE) is the difference in total energy between the ionized (E_+) and the neutral state (E_0). The relative shift in the BE, namely the core level shift, is then the difference with respect to the reference configuration: $\Delta BE = [E_+ - E_0] - [E_+^{ref} - E_0^{ref}]$. The total energy for the ionized system (E_+) is obtained by replacing the pseudopotential of a selected atom with another one, which simulates the presence of a screened core hole. Therefore, the BE shift of the core O1s level is approximated by differences in total energies calculated in supercells containing an excited O atom at different positions in the supercell, obtained via full relaxation of the electronic charge density, thus in conditions of complete static screening, the so-called final-state theory.[33] This approach does not allow us to fix the absolute values of the core levels but rather their relative shift. For a better comparison with the experimental data, spectra are aligned to the experimental value for the O_I peak (O in ZnO wurtzite at 531 eV).

Near-edge X-ray absorption fine structure (NEXAFS) spectra for oxygen K-edge were simulated by using the first-principles scheme based on the continued-fraction approach and ultrasoft pseudopotentials proposed by Ch. Gougoussis et al. and implemented in the Quantum ESPRESSO package.[34] Since defective ZnO and AZO systems include inequivalent oxygen atoms, we repeated the NEXAFS calculations for each oxygen in the simulation cell and we averaged the resulting spectra.

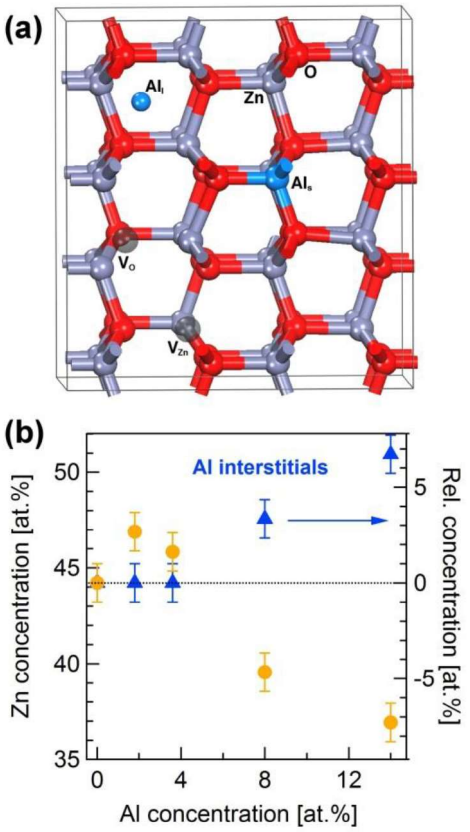

Fig. 1: (a) Atomic model of the AZO film, with the indication of dopants and vacancies sites in the lattice. (b) Zn concentration in AZO film as a function of Al dopant concentration measured by Zn3p/O1s ratio in HAXPES (dots). Right axis indicates the Zn variation with respect to the pure ZnO and the estimation of Al in interstitial sites as the difference between total Al and relative Zn concentration (triangles).

Results and discussion

AZO films of increasing dopant concentration from 0 to 14 at.% have been previously characterized by means of electrical, optical and electronic measurements.[12] This extended investigation has evidenced that the electrical resistivity, with its inversion point at 3.6 at.% (optimal doping condition), follows the core level shifts and CB population. Overdoping induces the depopulation of the CB and the appearance of additional electronic states in the gap. At low-medium concentration (< 3.5-4 at%) Al is easily incorporated as substitutional in a Zn site. This occurs both saturating existing Zn vacancies and replacing Zn atoms in the host, due to the rather low formation energy of the substitutional dopant.[13] In this configuration Al donates its 3p electron to the oxide highly dispersive conduction band and as a consequence the Fermi level shifts above the CB minimum as a function of dopant concentration. The material becomes then a highly degenerate n-type conductor and since undefective AZO does not insert any states in the bandgap, it preserves transparency.[11,14,16] At higher concentrations Al dopants occupy also interstitial sites. They introduce localized filled states with strong Al and O components in the gap and structural modifications in the crystal and are therefore responsible for the optical and electrical degradation of the material.[11,12] Increasing further the concentration above 20 at.% induces the formation of an homologous $(ZnO)_n(Al_2O_3)$ phase.[35] Since however we never reach these high concentrations and have no evidence of the appearance of new phases apart from ZnO wurtzite in XRD, we do not take this phase into consideration in our model.

Fig. 1a reports the atomic model assumed in this work. Al dopant positions are indicated both for substitutional and interstitial atoms, together with vacancy sites. Further details on the calculation of these defects and their DOS can be found elsewhere.[16] Fig. 1b reports the stoichiometry of the film determined from the Zn3p/O1s HAXPES ratio. The high photon energy used for the measurements characteristic of this technique allows us to conclude that this stoichiometry is indicative of the bulk composition of the film. Zn concentration is in principle expected to be 50 at.% in pure ZnO, while the whole curve is well below this ideal stoichiometry. This suggests that ZnO films are grown in conditions of excess O, producing most likely Zn vacancies (or O interstitials). Stoichiometry has an inversion point at about 2 at.% followed by a saturating slope. Initial Al doping at low concentration maintains an almost constant Zn:O ratio due to Al occupation

of V_{Zn}, while a further doping determines a reduction of Zn quantity, due to Al substitution. This slope tends to saturation, as Al interstitials are steadily introduced. However, while a decreasing slope is evident, saturation is not reached up to 14 at.%, suggesting that also at these high doping conditions part of the Al is still substituting Zn. The variation of Zn concentration is about -7 at.% with respect to undoped ZnO at 14 at% Al doping. We can infer that the remaining 7 at.% of Al atoms are located in interstitial sites, as obtained from the difference between the total Al concentration and the Zn variation with respect to undoped ZnO in the Zn:O stoichiometry (Fig. 1b). This curve shows that no Al interstitials are present below about 4 at.%, confirming the thermodynamic solubility limit reported in literature, defined as the concentration above which Al cannot be anymore entirely accommodated in substitutional sites.[35,36]

To investigate in more detail the film composition and the defects present in the film we have studied the HAXPES O1s lineshape. Fig. 2a shows the O1s measured for increasing dopant concentration. ZnO shows a narrow peak at 531 eV (O_I, associated with O in ZnO wurtzite matrix) with a small component at about 1.7 eV higher binding energy (more visible in the inset). This component is most likely not associated to the presence of surface OH, as it is expected at higher energy (about 2.2-2.5 eV from O_I). Furthermore, surface contamination contribution to spectrum is minimal in HAXPES, where for example no C is detected, and measurement is performed in normal emission. To give a qualitative evaluation the contribution to the photoemission spectrum of the first 2 Å with a standard X-ray source accounts for roughly 20% of the spectrum while here it is reduced to less than 10%. This allows to reduce drastically the contribution of surface contamination while in standard XPS this is always present in samples that have been exposed to air even for short time. Even more important in present experimental conditions the first 10 Å contribute with 40% of the HAXPES signal (compared to 70% for standard XPS), drastically reducing the possibility of assigning surface (or near-surface-region) properties to the bulk material.[37]

The addition of Al atoms to the ZnO matrix induces a modification of the O1s peak, that shifts to higher binding energy up to 4 at.% and then moves back to lower BEs (inset of Fig. 2b),[12] and shows a pronounced enlargement on the higher binding energies. Secondly, a slight enlargement is observed also on the low binding energy side of the main peak, especially above 3.6 at%. We have therefore fitted the O1s lineshape with three Gaussian components. The fit for the optimally doped sample is reported in Fig. 2b, together with the component relative areas of the obtained components.

Besides the main peak located at about 531 eV (O_I), a second Gaussian peak is located at about +0.6 eV from the main peak and is present in all doped samples (O_{II}). A third Gaussian (O_{III}) is necessary to take into account the enlargement at low binding energy, in order to maintain the values of the main peak (in terms of FWHM and position) and obtain an accurate fit. O_{III} is located about -0.5 eV BE with respect to the main

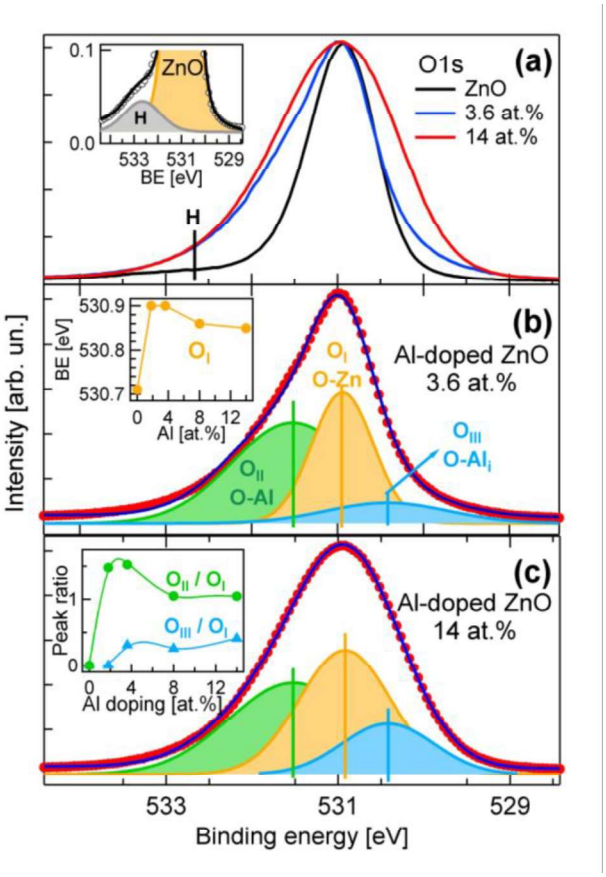

Fig. 2: (a) Normalized HAXPES O1s of AZO films with increasing Al concentration. Peaks have been aligned to the 3.6 at.% to better compare the lineshapes. Inset shows the zoom on the H contribution. (b-c) Gaussian fitting of the 3.6 and 14.2 at.% O1s respectively. Insets: peak position and area ratios of Gaussian components as obtained from the fitting procedure.

peak. O_{II} increases in intensity with increasing doping, while its FWHM slightly decreases. O_{III} is minimal for the optimally doped sample and increases for overdoping conditions. Besides the reduction in FWHM of O_{II} and O_{III}, main peak O_I broadens above the optimally doping condition (3.6 at.%). This could be assigned to the presence of additional components closer to the main peak (that cannot be disentangled). In TCO the availability of extra-charge free to screen the core hole left by the photoemission process in the final state can give rise to satellite peaks, as reported for SnO_2 and In_2O_3.[38,39] In the present case this contribution can be ruled out, based on previous work on core levels, where no significant extra satellites were reported on Zn3p peaks.[12]

In order to decouple the effect of dopants and defects in our samples, we simulated the O1s core level spectra for different and controlled configurations, as displayed in Figure 3. Panel (a) shows the O1s lineshape for defective ZnO bulk, in the absence of Al dopant. While the presence of oxygen vacancies (V_O) does not modify the pristine O contribution in ZnO wurtzite matrix (O_I), the inclusion of Zn vacancies (V_{Zn}) perturbs the local chemical environment of the four next-neighbour O atoms, giving rise to two further contributions at +0.3 eV and -1.3 eV, respectively. Interstitial oxygens (O_i) insert an extra low-intensity peak at +0.4 eV, almost degenerate with

the tail of the V_{Zn} contribution, preventing an unambiguous discrimination between the two effects. Finally, the inclusion of H atoms, bonded to oxygen of the host, is responsible for a separate peak at +1.7 eV. This is in very good agreement with the experimental analysis, where the component is clearly observed in undoped ZnO, evidencing H incorporation.

Figure 3b shows the calculated O1s lineshape for undefective Al:ZnO, for increasing amount of Al dopant. In the sub-solubility regime (< 3.5 at.%) Al is included only as Zn substitutional dopant (Al_{Zn}). Since Al_{Zn} are four-fold coordinated only to oxygen atoms, we can easily distinguish between oxygens bonded to Zn or to Al species. This is responsible for the appearance of a second contribution at +0.6 eV in quantitative agreement with the experimental detection of peak O_{II}. Increasing the amount of substitutional dopants simply changes the relative intensity of O_I and O_{II} peaks. On the contrary, the presence of interstitial Al impurities strongly modifies the lineshape of the spectrum shifting the position of O_{II} peak at +0.4 eV and introducing two extra peaks at -0.3 eV and -1.1 eV, respectively, that match O_{III} peak observed in HAXPES.

When both dopants and defects are simultaneously taken into account, the spectral features of the single characters generally sum up, as shown in Figure 3c. Here, we can easily recognize the O_I - O_{II} peak split due to the presence of Al impurity, as well as the peak at -1.3 eV, which is the fingerprint

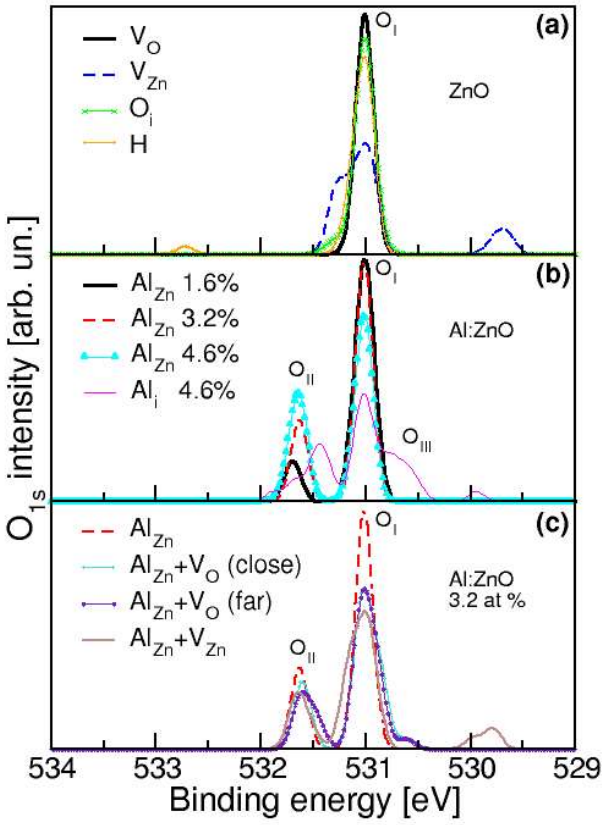

Fig. 3. Simulated O1s core level spectra for (a) defective ZnO in the absence of Al dopant; (b) undefective Al:ZnO at different Al content; (c) defective Al:ZnO for 3.2 at%. All spectra are shifted to the experimental O_I value, for clarity.

of the zinc vacancy. Two different structures were considered for the case of oxygen vacancies: in one case (labelled far) the oxygen is removed from the ZnO host far away from the Al impurity, in the other (labelled close) the removed oxygen would be bonded to aluminium; in the former case the Al ion is tetra-coordinated, in the latter it is ter-coordinated with next-neighbour oxygens. Their spectral features are very similar to the undefective case, except for a low-intensity peak at -0.4 eV, which superimposes to the interstitial contribution to peak O_{III}, discussed in Fig. 2b. Summarizing, through the comparison with experimental results, we can unambiguously assign peak O_I to the pristine oxygen contribution from ZnO host and O_{II} to the presence of substitutional Al dopants. Peak O_{III} is mainly due to Al interstitial, that increase in intensity consistently with the concentration estimated by stoichiometry (Fig. 1). Point defects in the host (V_O, V_{Zn}, O_i, H) hardly modify this scenario, while they are mainly responsible for a broadening of the spectrum, as detected by the experiments. Finally, the absence of a high-intensity contribution at -1.3 eV in the experimental spectrum confirms the good quality of the sample and the relative low presence of Zn vacancies during growth. We cannot however exclude that a small quantity of V_{Zn} and O_i are present below the sensitivity of HAXPES, supporting the low conductivity value reported in previous work in spite of the H presence.[12]

NEXAFS measurements were performed by total electron yield for Al-doped ZnO in the 0-14 at.% Al concentration, both at the energy range of the Oxygen K-edge and the Zinc $L_{2,3}$-edge (Fig. 4). The NEXAFS O K-edge can be used to follow the evolution of chemical state of the O atoms in the ZnO matrix as a function of the Al content. O K-edge for pure ZnO thin film and for Al doped film with increasing Al concentration are displayed in Fig.4a. From the available literature, the broad spectral features between 530 and 539 eV are assigned to the hybridization between the O 2p and the Zn 4s states, forming the bottom of the conduction band.[18,23,40,41] The sharp peak at around 537 eV is due to the transition of O 1s electrons to more localized $O2p_z$ and $2p_{x+y}$ states. At higher energies, the features between 539 and 547 eV are due to the transitions to the states formed due to the hybridization between the O 2p states with the Zn 4p states. The absence of pre-edge peaks - typical of the hybridization between the O 2p and the transition metal 3d states - is the confirmation that the Zn in all films (included those with high Al concentration) are in a $3d^{10}$ configuration.[42] In the present work the O K-edge of the undoped ZnO sample is in perfect agreement with literature.[18] The shape of the spectrum gradually changes as a function of the Al content going from a spectrum with many well defined structures to a more smooth and structureless spectrum for the most doped (14 at.% Al) samples. This behaviour is typically correlated with metallicity because transition metal oxide spectra are in general more structured than their metal counterparts. However here it is more likely associated with the crystalline quality or the presence of structural defects. In fact, the conductivity of the sample grows from 0 at% to 3.6 at% but then drops dramatically after 5 at% doping while the spectra continuously change from 0 to 14 at% Al content, with

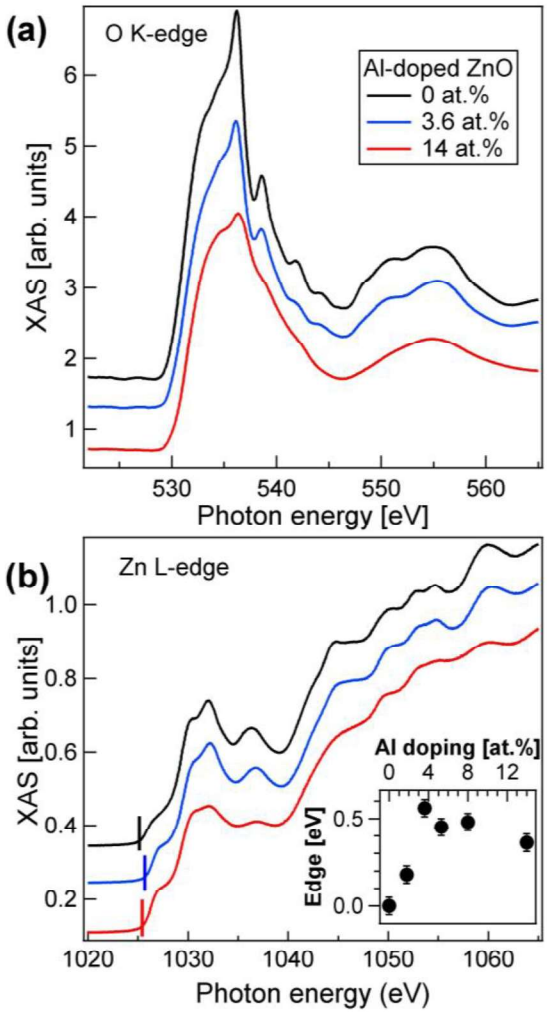

Fig. 4: X-ray absorption spectra of (a) O K–edge and (b) Zn $L_{2,3}$ –edge measured by total electron yield. Inset shows the shift of the Zn L white line with respect to ZnO.

a more rapid modification of the lineshape for Al concentration above 3.6 at%, which represents the solubility limit of the Al in the ZnO matrix. On the Zn L-edge (Figure 4b) we observe the same behaviour (a smoothing of the lineshape of the spectra as a function of the Al doping), even if less pronounced than observed on the O K-edge. Moreover, due to the shift of the bottom of the conduction band as a function of the Al doping, the onset of the absorption of the Zn L white line shifts accordingly (inset of Fig. 4).[12]

Figure 5 displays the simulated Oxygen K-edge XAS spectra for ZnO and Al:ZnO compounds. Zero energy is set to the Fermi level of ZnO crystalline bulk (grey area). Four main peaks (A-D) dominate the lowest energy part of the spectrum. The shape and the energy distribution of these peaks accurately reproduce the experimental findings of Figure 3a, in excellent agreement with previous theoretical simulations.[18]

In panel (a) we superimpose the projected density on 2p states of the excited O* atoms (crossed shaded area), i.e. the one including the core-hole, as well as the 4s Zn atom contribution. This confirms the assignment of the peaks A-C (corresponding to 530-540 eV in the experimental spectra) to electron transitions from O1s to O2p, which are broadly hybridized with the 4s states of Zn at the bottom of the ZnO conduction band.

The effect of Al doping is reported in panel (b). The inclusion of Al imparts a semiconductor-to-metal transition to the systems.[10,16] The increase of the Al content corresponds to an upward shift of the Fermi level with respect to the bottom of the conduction band of pristine ZnO bulk, consistent with the experiment. Coherently, the as-simulated XAS spectra result to be shifted one to the other as the corresponding Fermi levels. In panel (b) we realigned the spectra to the Fermi energy of ZnO in order to better highlight the modifications to peaks A-D, caused by the dopant.

The progressive inclusion of Al dopant in Zn substitutional sites (from 1.6 to 4.6%) causes a systematic quenching of peak B and the slight increase of peak C, as shown in inset 1 of panel (b). The increasing of Al content further fills the valley between peaks C and D (see inset 2). More visible is the effect of interstitial Al dopants that strongly reduces the intensity of peaks B, C and D giving rise to a less structured spectrum. This confirms the trend observed in Figure 4a, which corresponds to a progressive broadening and flattening of spectra as a

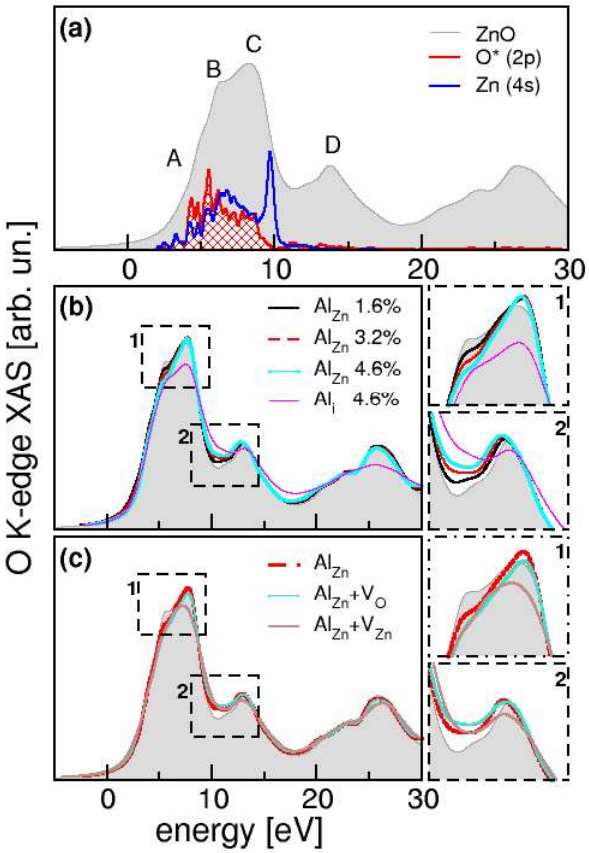

Fig. 5. Simulated Oxygen K-edge XAS spectra for (a) undefective ZnO wurtzite; (b) undefective Al:ZnO at increasing Al content; (c) defective Al:ZnO at 3.2 at %. ZnO spectrum (grey area) is reported in all panels as a reference. Panel (a) includes also the projected-density of states on 2p orbitals of the excited oxygen atom O (red crossed area) and Zn4s orbitals (blue line). Lateral insets (1, 2) in panels b and c show zooms on specific section of overall spectra. Zero energy is set to Fermi level of pristine ZnO bulk.*

function of the increase of Al content. Broadening of Zn L-edge is therefore less pronounced due to next-nearest neighbour position of Zn with respect to Al.

The presence of dopants and defects further complicate this scenario, as shown in Figure 5c, where the undefective spectra for ZnO (grey area) and Al:ZnO (dashed red line) are reported as a reference. Irrespective of the proximity to Al dopant, oxygen vacancies slightly perturb the main features of the spectrum, while Zn vacancies cause a remarkable reduction of peaks B, C and D. This confirms the role of Zn4s states in the spectral distribution of final states O*2p, discussed above (panel a).

The powerful combination of DFT and X-ray spectroscopies have allowed to determine clearly the defects present in the film, their sites and their contribution to the overall electric and optical properties. These methods have proven to be a valuable way to control and thus improve efficiently the quality of the material. Combined with a good control of deposition methods, this can lead to TCO films with controlled conductivity and mobility, larger carrier density and designed optical response, in terms of transparency and plasmonic frequency.

Conclusions

By means of HAXPES and NEXAFS spectra of O lines we have shown that undoped ZnO grown by sputter deposition has H as the only defect contributing to conductivity, while a significant contribution of Zn vacancies can be excluded. When the oxide is doped with an increasing amount of Al up to 3.5 at.%, impurity atoms sit in substitutional sites, introducing a new intense component in O1s peak and slightly modifying the relative intensity in main features of O K-edge. When Al starts sitting in interstitial sites a third small component is added in O1s, together with a broadening of the main wurtzite peak and of the NEXAFS structures, indicative of the increased coordination of Oxygen neighbours and local lattice distortions.

This study demonstrates how the simultaneous presence of defects and impurities gives rise to a very complex spectroscopic plot, even in the case of simple binary materials, such as wurtzite ZnO. Local geometrical distortions, stoichiometry deviations and compensation effects compete and impart a unique behavior to the system. The combination of X-ray spectroscopic investigation of electronic response in AZO films combined with their theoretical interpretation allowed us to identify the single chemical and structural contributions that give origin to the final properties of the samples. Analogous studies can be applied to a series of materials of interest for optoelectronics (other TCOs, nitrides,…), opening the way to a deeper understanding of the material behavior (in terms of conductivity, carrier density, trapping sites, donor-acceptor levels available) and of material control, in order to properly tune their response and to realize innovative and reproducible devices.

Conflicts of interest

There are no conflicts to declare.

Acknowledgements

Authors would like to acknowledge the PRIN Project 2015CL3APH – NEWLI financed by MIUR for the financial support. This work has been partly performed in the framework of the Nanoscience Foundry and Fine Analysis (NFFA MIUR Italy Progetti Internazionali). We acknowledge SOLEIL for provision of synchrotron radiation facilities, and we would like to thank Denis Céolin for assistance in using Galaxies beamline.

References

1 Eds. K. Ellmer, A. Klein, B. Rech. *Transparent Conductive Zinc Oxide.* s.l. : Springer Series in Material Science 104, 2008.
2 G. V. Naik, V. M. Shalaev and A. Boltasseva, *Adv. Mater.* 2013, **25**, 3264.
3 P. D. C. King and T. D. Veal, *J. Phys.: Condens. Matter.* 2011, **23**, 334214.
4 J. E. Stehr, K. M. Johansen, T. S. Bjørheim, L. Vines, B. G. Svensson, W. M. Chen and I. A. Buyanova, *Phys. Rev. Applied.* 2014, **2**, 021001.
5 A. Janotti and C. G. Van de Walle, *Phys. Rev. B.* 2007, **76**, 165202.
6 D. C. Look, G. C. Farlow, P. Reunchan, S. Limpijumnong, S. B. Zhang and K. Nordlund, *Phys. Rev. Lett.* 2005, **95**, 225502.
7 C. G. Van de Walle, *Phys. Rev. Lett.* 2000, **85**, 1012.
8 S. Benedetti, N. Nilius, S. Valeri, S. Tosoni, E. Albanese and G. Pacchioni, *J. Phys. Chem. C.* 2016, **120**, 13604.
9 A. Stadler, *Materials* 2012, **5**, 661.
10 A. Calzolari, A. Ruini and A. Catellani, *ACS Photonics* 2014, **1**, 703-709.
11 M. Bazzani, A. Neroni, A. Calzolari and A. Catellani, *Appl. Phys. Lett.* 2011, **98**, 121907.
12 I. Valenti, S. Benedetti, A. di Bona, V. Lollobrigida, A. Perucchi, P. Di Pietro, S. Lupi, S. Valeri and P. Torelli, *J. Appl. Phys.* 2015, **118**, 165304.
13 S. Lany and A. Zunger, *Phys. Rev. Lett.* 2007, **98**, 045501.
14 J. G. Lu, Z. Z. Ye, Y. J. Zeng, L. P. Zhu, L. Wang, J. Yuan, B. H. Zhao and Q. L. Liang. *J. Appl. Phys.* 2006, **100**, 073714.
15 J. T-Thienprasert, S. Rujirawat, W. Klysubun, J. N. Duenow, T. J. Coutts and S. B. Zhang, *Phys. Rev. Lett.* 2013, **110**, 055502.
16 A. Catellani, A. Ruini and A. Calzolari, *J. Mater. Chem. C.* 2015, **3**, 8419-8424.
17 J. Y. Noh, H. Kim, Y. S. Kim and C. H. Park, *J. Appl. Phys.* 2013, **113**, 153703.
18 C. Guglieri and J. Chaboy, *J. Phys. Chem. C.* 2014, **118**, 25779-25785.
19 K. Nomura, T. Kamiya, E. Ikenaga, H. Yanagi and K. Kobayashi, J. *Appl. Phys.* 2011, **109**, 073726.
20 J. C. C. Fan and J. B. Goodenough, *J. Appl. Phys.* 1977, **48**, 3524.
21 M. Chen, X. Wang, Y.H. Yu, Z.L. Pei, X.D. Bai, C. Sun, R.F. Huang and L.S. Wen, *Appl. Surf. Sci.* 2000, **158**, 134.
22 M. Gabàs, P.Dıàz-Carrasco, F.Agullò-Rueda, P.Herrero, A.R. Landa-Cànovas and J.R.Ramos-Barrado, *Sol. Energy Mater. Sol. Cells.* 2011, **95**, 2327-2334.
23 J. G. Chen, *Surf. Sci. Rep.* 1997, **30**, 1-152.

24 D. Céolin, J.M. Ablett, D. Prieur, T. Moreno, J.-P. Rueff, T. Marchenko, L. Journel, R. Guillemin, B. Pilette, T. Marin and M. Simon, *J. Electr. Specrosc. Relat. Phenom.* 2013, **190**, 188.
25 J.-P. Rueff, J. Ablett, D. Céolin, D. Prieur, T. Moreno, V. Balédent, B. Lassalle-Kaiser, J. Rault, M. Simon and A. Shukla, *J. Synchrotron Radiat.* 2015, **22**, 175.
26 G. Panaccione, I. Vobornik, J. Fujii, D. Krizmancic, E. Annese, L. Giovanelli, F. Maccherozzi, F. Salvador, A. De Luisa, D. Benedetti, et al. *Rev. Sci. Instrum.* 2009, **80**, 043105.
27 P. Giannozzi, S. Baroni, N. Bonini, M. Calandra, R. Car, C. Cavazzoni, D. Ceresoli, G. L. Chiarotti, M. Cococcioni, I. Dabo, et al. QUANTUM ESPRESSO: a modular and open-source software project for quantum simulations of materials. *J. Phys. Condens. Matter.* 2009, **21**, 395502. See also www.quantum-espresso.org.
28 J. P. Perdew, K. Burke and M. Ernzerhof, *Phys. Rev. Lett.* 1996, **77**, 3865-3868.
29 M. Korotin, T. Fujiwara and V. Anisimov, *Phys. Rev. B* 200, **62**, 5696.
30 S. G. Park, B. Magyari-Köpe and Y. Nishi, *Phys. Rev. B* 2010, **2**, 115109.
31 L. A. Agapito, S. Curtarolo and M. Buongiorno Nardelli, *Phys. Rev. X.* 2015, **5**, 011006.
32 P. Gopal, M. Fornari, S. Curtarolo, L. A. Agapito, L. S. I. Liyanage and M. Buongiorno Nardelli, *Phys. Rev. B.* 2015, **91**, 245202.
33 E. Pehlke and M. Scheffler, *Phys. Rev. Lett.* 1993, **71**, 2338-2341.
34 C. Gougoussis, M. Calandra, A. P. Seitsonen and F. Mauri, *Phys. Rev. B.* 2009, **80**, 075102.
35 S. Yoshioka, F. Oba, R. Huang, I. Tanaka,T. Mizoguchi and T. Yamamoto, *J. Appl. Phys.* 2008, **103**, 014309.
36 M. H. Yoon, S. H. Lee, H. L. Park, H. K. Kim and M. S. Jang, *J. Mater. Sci. Lett.* 2002, **21**, 1703.
37 G. Panaccione, F. Offi, M. Sacchi and P. Torelli, *C. R. Physique.* 2008, **9**, 524.
38 C. Körber, V. Krishnakumar, A. Klein, G. Panaccione, P. Torelli, A. Walsh, J. L. F. Da Silva, S.-H. Wei, R. G. Egdell and D. J. Payne. *Phys. Rev. B.* 2010, **81**, 165207.
39 R. G. Egdell, J. Rebane, T. J. Walker and D. S. L. Law, *Phys. Rev. B.* 1999, **59**, 1792.
40 S. Krishnamurthy, C. McGuinness, L. S. Dorneles, M. Venkatesan, J. M. D. Coey, J. G. Lunney, C. H. Patterson, K. E. Smith, T. Learmonth, P.-A. Glans, T. Schmitt and J.-H. Guo, *J. Appl. Phys.* 2006, **99**, 08M111.
41 A. P. Singh, R. Kumar, P. Thakur, N. B. Brookes, K. H. Chae and W. K. Choi, *J. Phys. Condens. Matter.* 2009, **21**, 185005.
42 D. H. Douma, R. Ciprian, A. Lamperti, P. Lupo, E. Cianci, D. Sangalli, F. Casoli, L. Nasi, F. Albertini, P. Torelli and A. Debernardi, *Phys. Rev. B.* 2014, **90**, 205201.